

Long Shutdown 2 developments at REX/HIE-ISOLDE for improved ion beam characterization and manipulation

Niels Bidault^{1,2}, Jose Alberto Rodriguez¹.

¹BE-OP-ISO, CERN, 1211 Geneva 23, Switzerland

²University of Rome ‘La Sapienza’ & INFN, 00185 Rome, Italy



SAPIENZA
UNIVERSITÀ DI ROMA

Contents

Introduction

REX/HIE-ISOLDE experimental overview

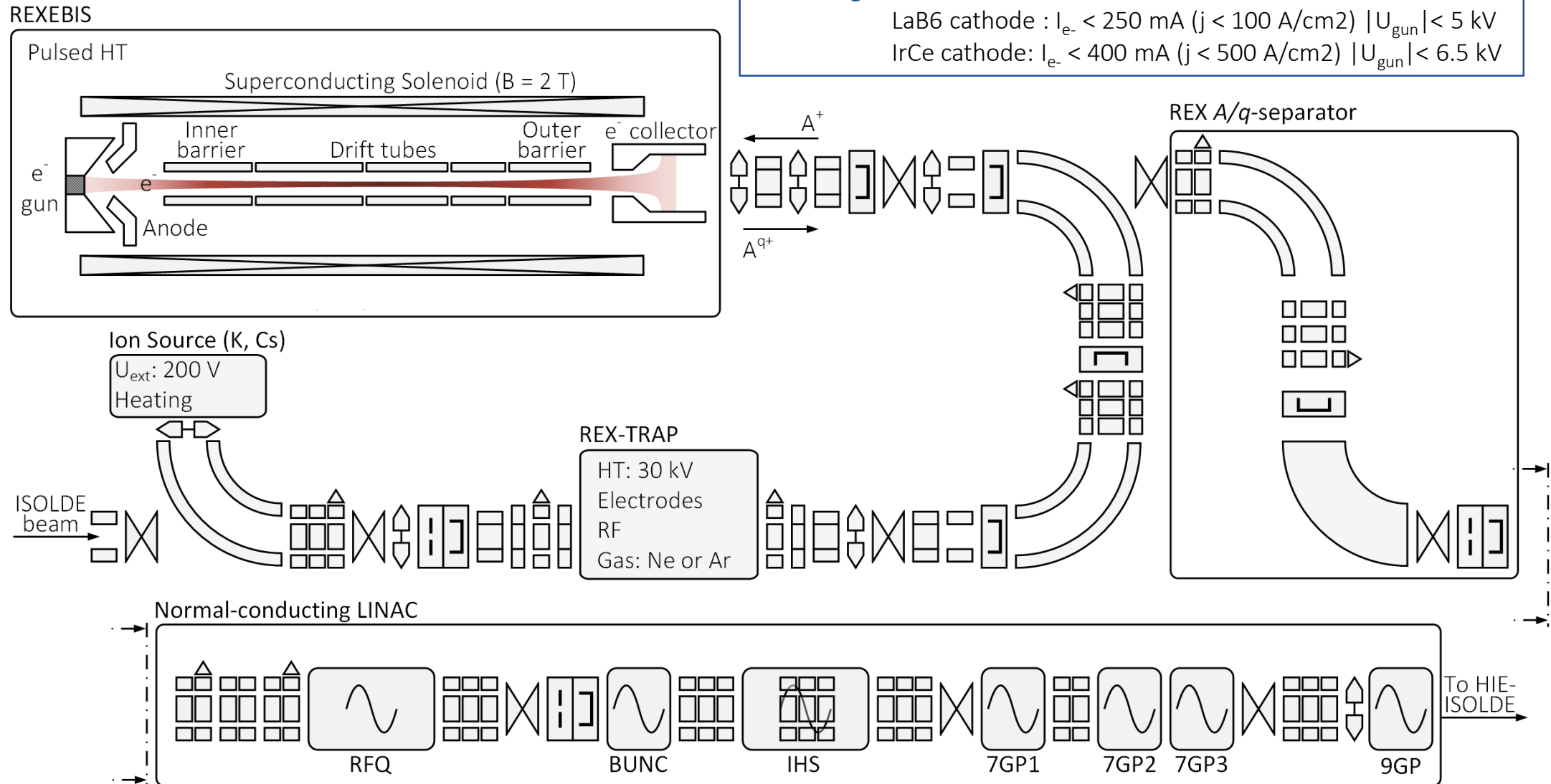
REXBIS developments

Non-adiabatic immersed gun
From abundant A/q-spectra to single-ion detection
Axial energy distribution

HIE-ISOLDE developments

Transverse beam properties
Beam energy distribution
Longitudinal phase-space characterization

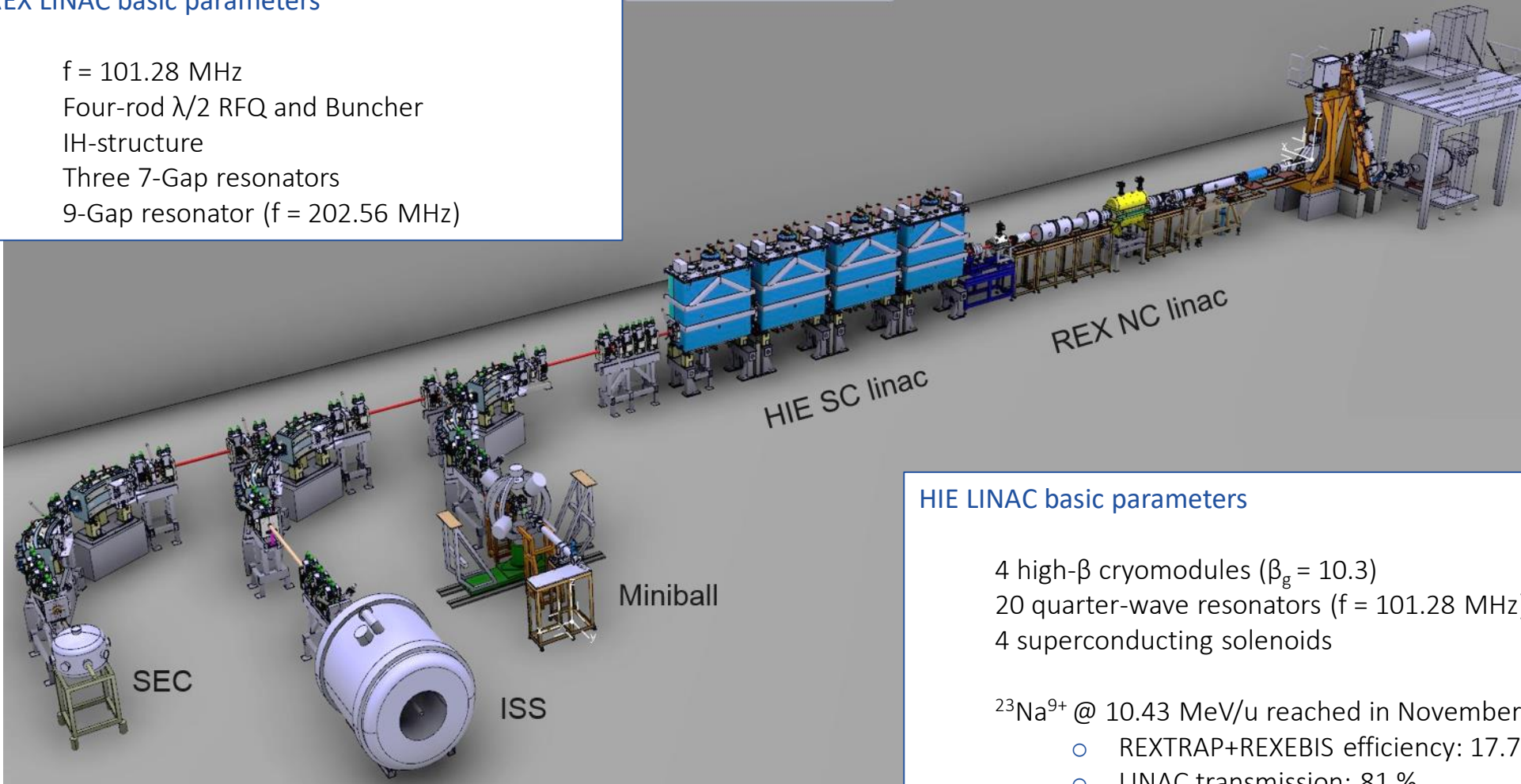
REX-ISOLDE



HIE-ISOLDE

REX LINAC basic parameters

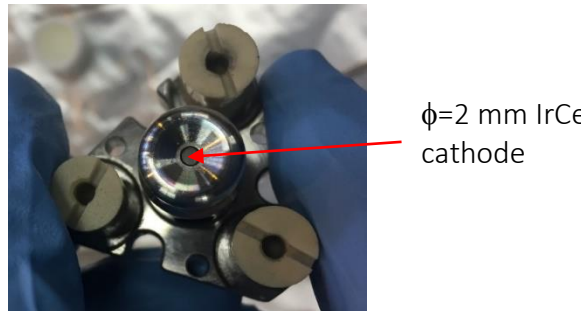
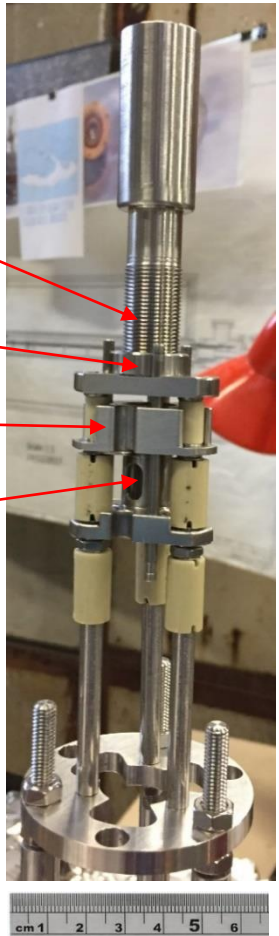
$f = 101.28$ MHz
Four-rod $\lambda/2$ RFQ and Buncher
IH-structure
Three 7-Gap resonators
9-Gap resonator ($f = 202.56$ MHz)



Non-adiabatic immersed electron gun

(Gunn Khatri's slide)

Design



Post anode used to adjustment the phase of cyclotron wrt iron ring for different beam currents

Results

Current and losses

I_e well behaved to 300 mA
<15 uA anode losses
<100 uA losses on drift tube in front of suppressor

EBIS breeding efficiency

19.7% for $^{39}\text{K}^{1+}$ to $^{39}\text{K}^{10+}$
Almost as high as for old gun

Effective current density

$T_{\text{breed}}=44\text{ ms}$ for $^{133}\text{Cs}^{1+}$ to $^{133}\text{Cs}^{31+}$
 j_e estimated to $\sim 400\text{ A/cm}^2$

Problems

1. Excessively high cathode work function (activation not helpful)
2. Electron beam losses rises exponentially when $I_e > 300\text{ mA}$. Believed to be caused by back-scattered or elastically reflected electrons from the collector region.

A. Pikin et al., "A method of controlling the cyclotron motion of electron beams with a non-adiabatic magnetic field", accepted PRAB

Abundant contamination

Technique Variation of REX A/q-Separator magnet, monitoring of current passing through slit on Faraday cup.

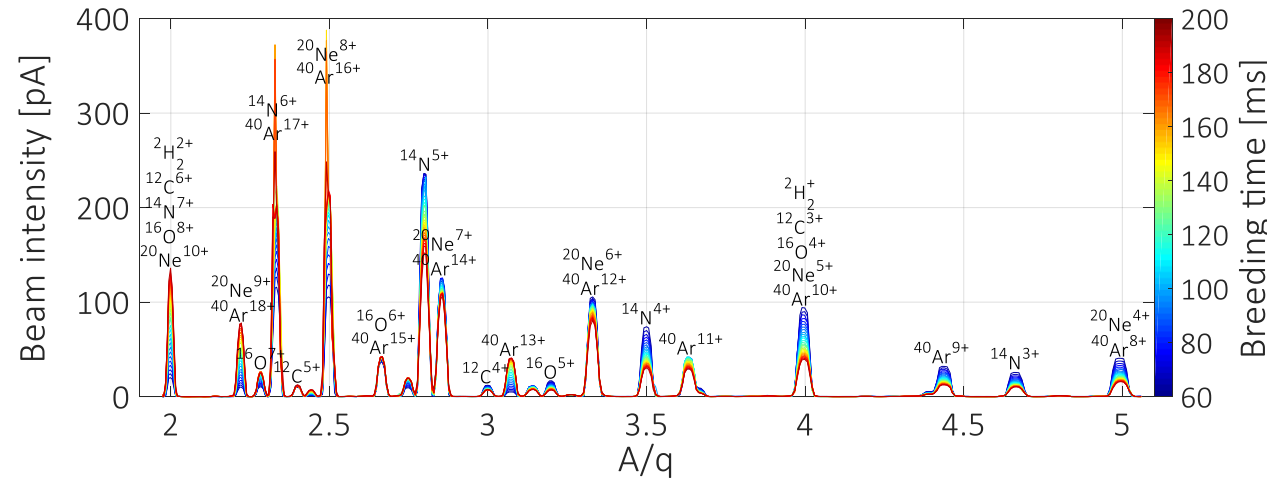


Figure Spectra obtained with previous immersed electron gun design, LaB6 cathode at $I_{e^-} = 200$ mA and $U_{\text{gun}} = 4$ kV (2017).

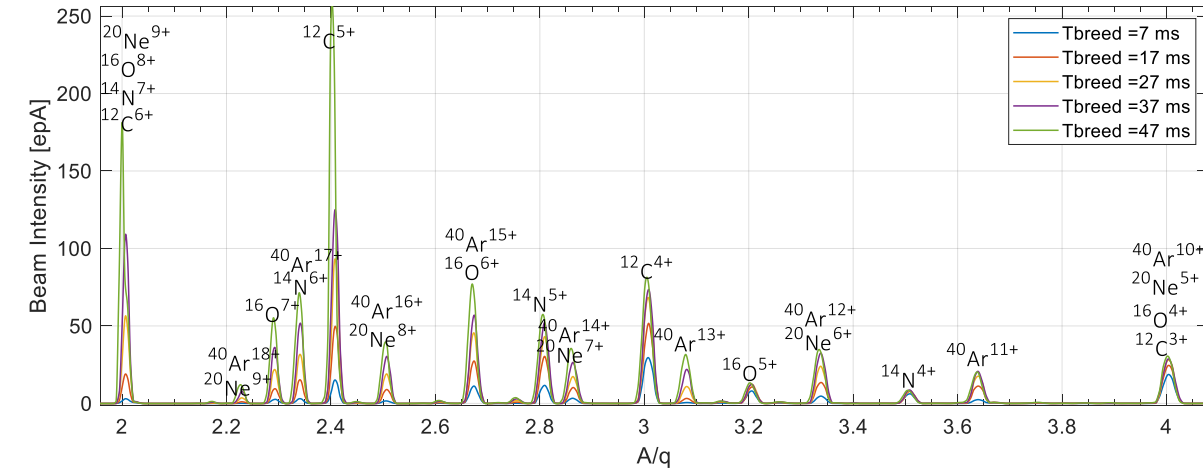


Figure Spectra obtained using non-adiabatic immersed electron gun, IrCe cathode at $I_{e^-} = 200$ mA and $U_{\text{gun}} = 6$ kV (2020).

- Expected contamination from air.
(Not labelled: ^{13}C , ^{15}N , ^{17}O , ^{18}O , ^{21}Ne , ^{22}Ne , ^{36}Ar , ^{38}Ar)
- Insights at the initial partial pressures of the components.

$$\text{Charge dynamics } \frac{dN_q}{dt} = \frac{j_e}{e} (N_{q-1} \sigma_{q-1}^{\text{EI}} - N_q \sigma_q^{\text{EI}}) + N_{q+1} \sigma_{q+1}^{\text{RR}} - N_q \sigma_q^{\text{RR}} + N_{q+1} \sigma_{q+1}^{\text{DR}} - N_q \sigma_q^{\text{DR}}$$

Electron impact ionisation
 Radiative recombination
 Dielectronic recombination
 +
 +
 +
 Charge exchange Escape rate

EBISIM - EBIS/T charge dynamics and plasma simulations

EBISIM package, collection of tools for simulating the evolution of the charge state distribution inside an Electron Beam Ion Source / Trap (EBIS/T) using Python –
Hannes PAHL

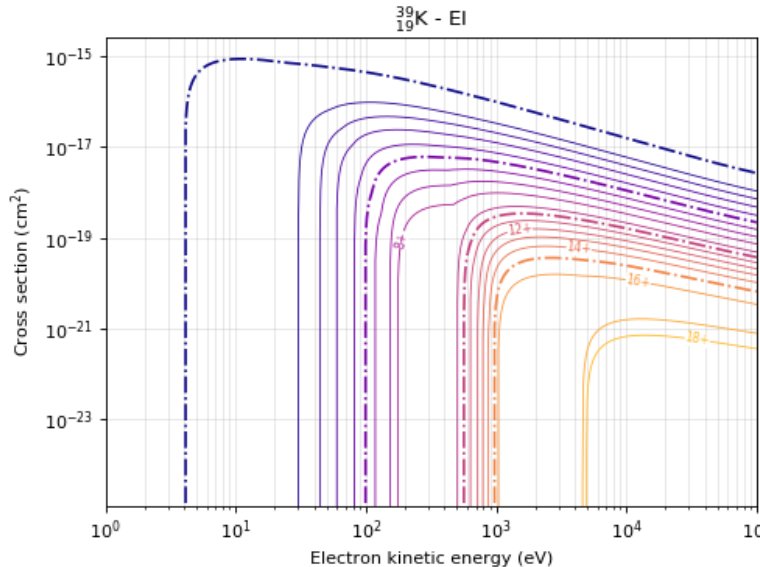


Figure Cross sections for electron impact ionisation (EI).

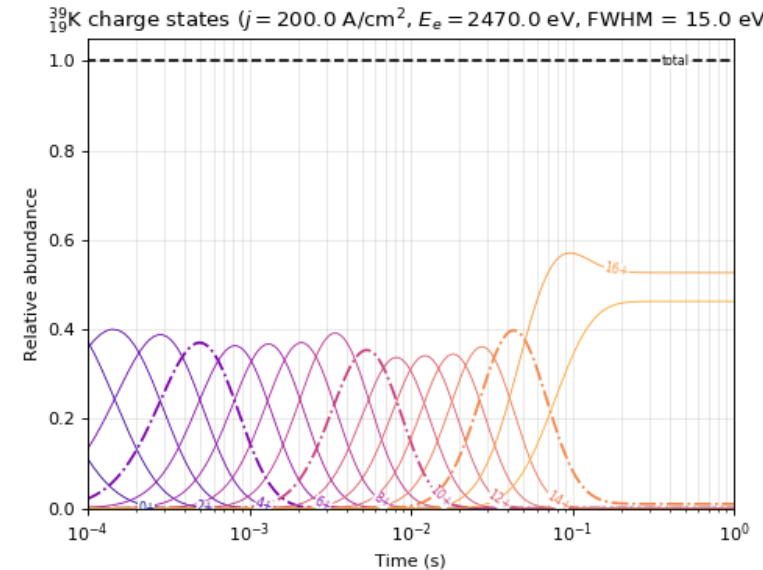


Figure Distributions of charge states of time for injected 1^+ beam (EI, RR and DR).

$$\text{Average potential seen } \langle \phi_i(kT) \rangle = \frac{\int q\phi\rho_i}{\int \rho_i}$$

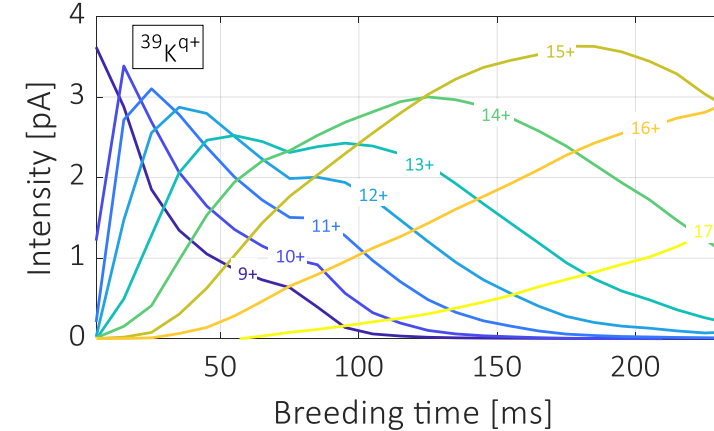
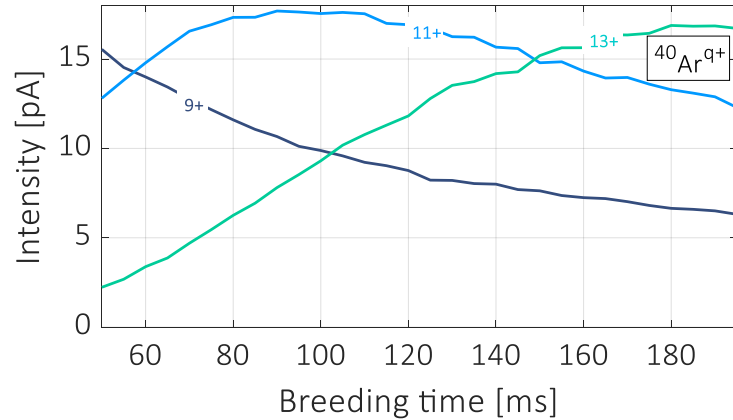
$$\text{Overlap factor } f(e, i)$$

$$\text{Heat capacity } C_v = \frac{d\langle \phi(kT) \rangle}{dkT} = \frac{n_{\text{DoF}}}{2}$$

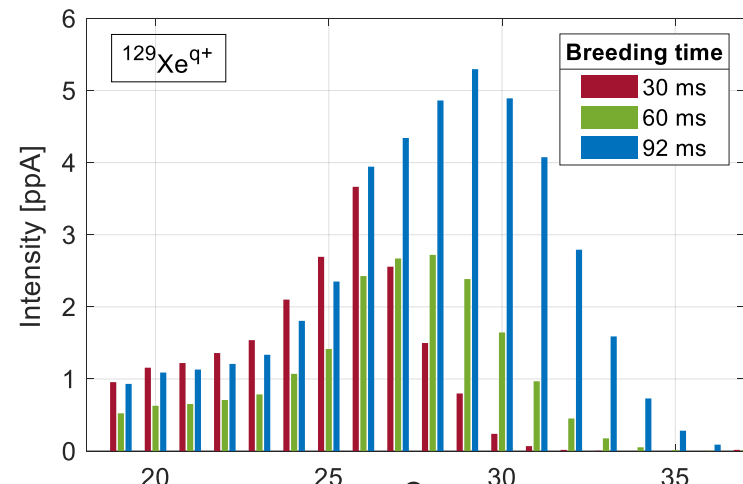
Useful links:

[Documentation](https://ebisim.readthedocs.io/en/latest/) (<https://ebisim.readthedocs.io/en/latest/>)
[GitHub](https://github.com/HPLegion/ebisim#readme) (<https://github.com/HPLegion/ebisim#readme>)

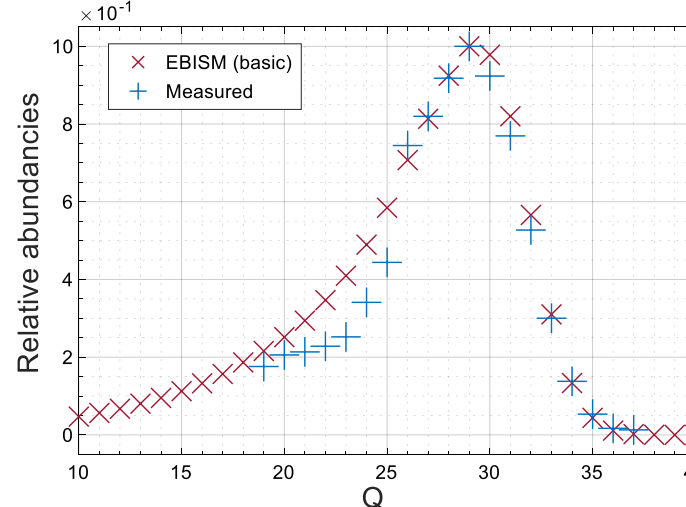
Charge state distributions



Figures Charge-state evolution as a function of breeding time for ionized residual gas (^{40}Ar) and injected beam (^{39}K).



Figures CS distributions using $I_{e^-} = 200 \text{ mA}$ for Xe^{q+} and comparison with simulations.



Estimate of j_{eff} , effective electron charge density, when comparing measured charge state distributions with EBISIM.

Pronounced discrepancies from expected j_{eff} when the injection of the beam into REXEBIS is not optimized with care.

Fitting results between EBISIM and measurement:

- $j_{\text{eff}} = 400 \text{ A/cm}^2$ for $I_{e^-} = 300 \text{ mA}$
- $j_{\text{eff}} = 300 \text{ A/cm}^2$ for $I_{e^-} = 200 \text{ mA}$

From epA to single-ion detection

Technique Instead of varying REX A/q-Separator magnet, all necessary beam optics and RF, from REXEBIS to the Si detector, are scaled for each A/q step.

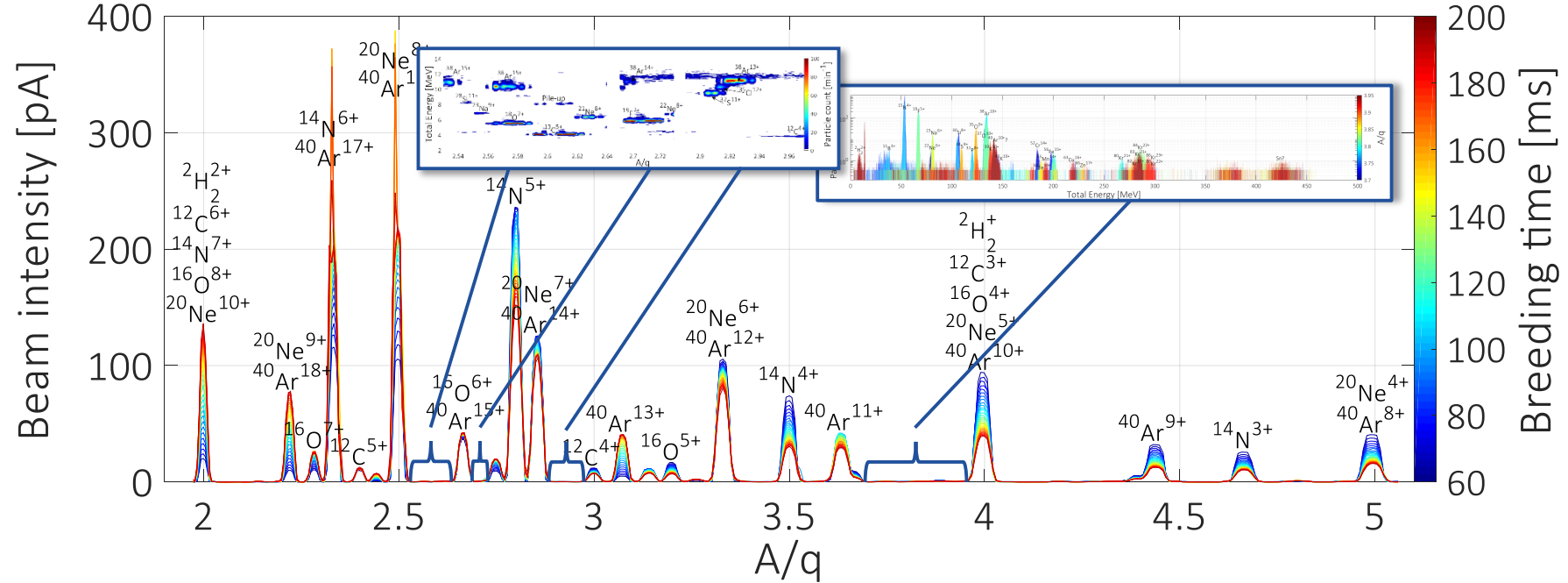


Figure Areas probed during the first tests for the conceptual proof of the method in 2017/2018.

Experimental setup in 2017/2018, using LaB6 cathode at lower electron beam density:

- Demonstration of the capability to probe rare contaminants.
- Residual gas ions were accelerated through the RFQ and transported to a Si detector.
- Intensities were not representative of reality.

From epA to single-ion detection

Results Obtained in 2017/2018 to evaluate the efficiency of probing rare contaminants across the A/q-spectra using a silicon detector.

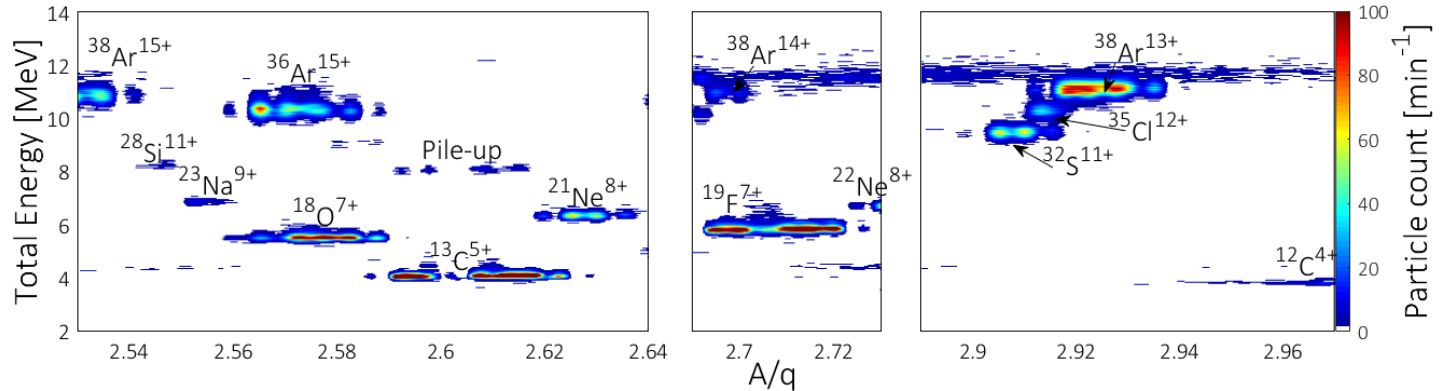


Figure Contour of energy histograms acquired on 9 mm-SD. Beam defocused. RR = 20 Hz; breeding time = 10 ms; I_{e^-} = 160 mA.

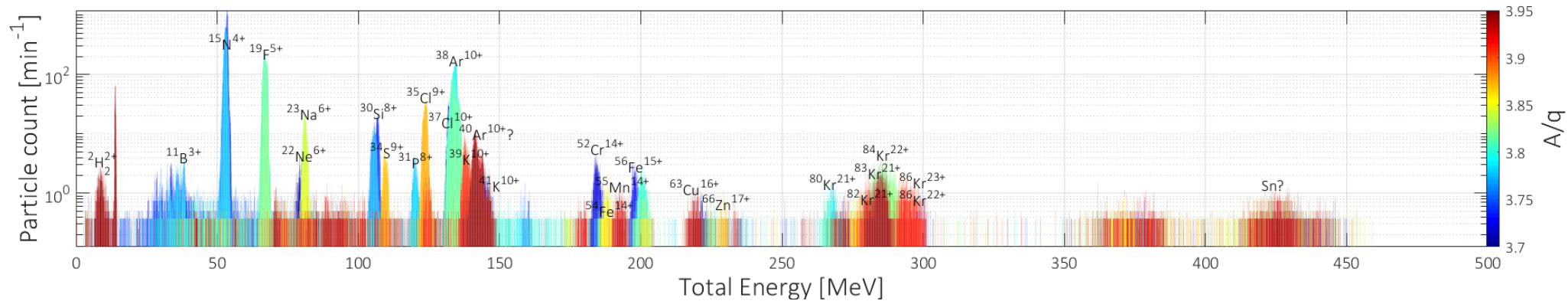


Figure Energy histograms acquired on 15 mm-SD. Foil 5%. RR = 20 Hz; breeding time = 35 ms; I_{e^-} = 140 mA.

"Residual Gas Ions Characterization from the REXEBIS", N. Bidault, *et al.*, IPAC2018, Vancouver, 10.18429.

From epA to single-ion detection

Technique Instead of varying REX A/q-Separator magnet, all necessary beam optics and RF, from REXEBIS to the Si detector, are scaled for each A/q step.

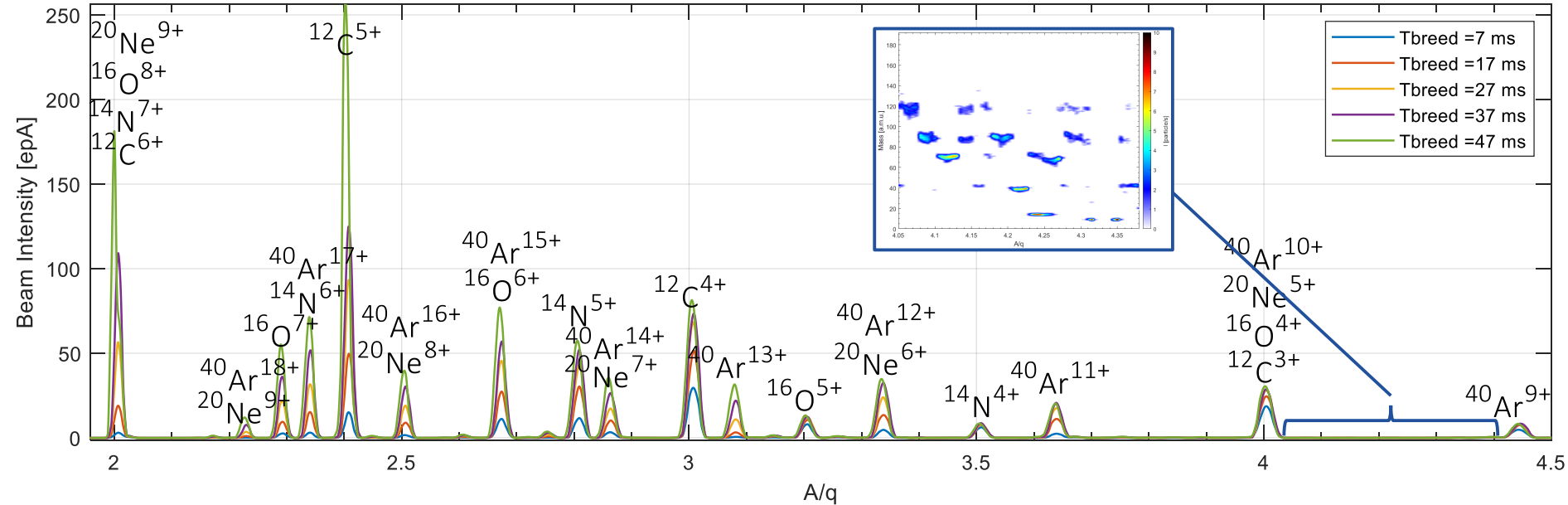


Figure Areas probed during the second batch of tests with new diagnostic boxes installed, in 2020.

Experimental setup in 2020, using non-adiabatic gun with IrCe cathode at higher electron beam density:

- Confirmation of the capability to probe rare contaminants.
- Residual gas ions were accelerated through the RFQ and acquired on a large Si detector installed directly afterward.
- Intensities are representative of reality.

Rare contaminants

Preliminary results/treatment

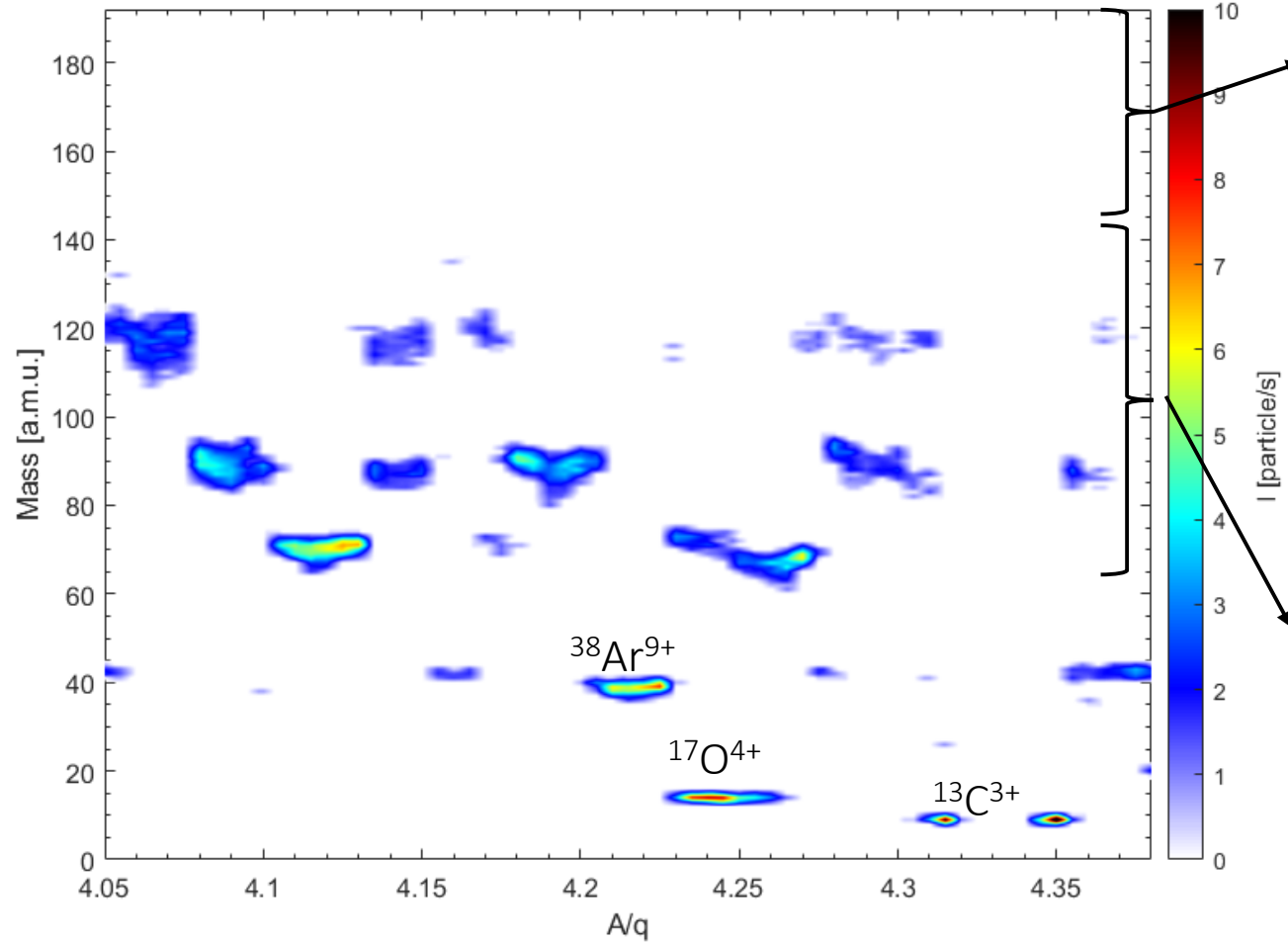


Figure Mass-scan measured with Breeding time = 45 ms; I_{e^-} = 250 mA.

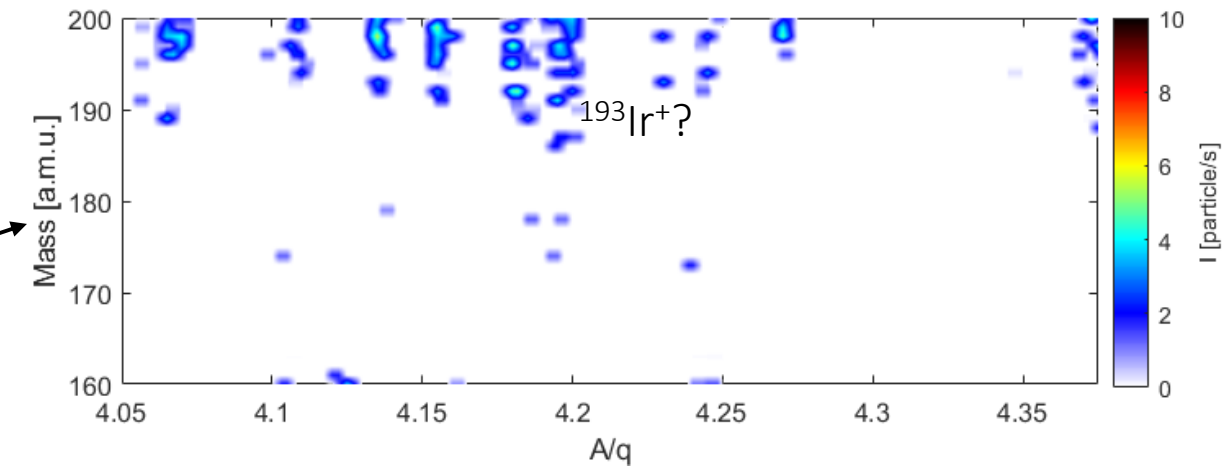


Figure Breeding time = 195 ms ; I_{e^-} = 250 mA.

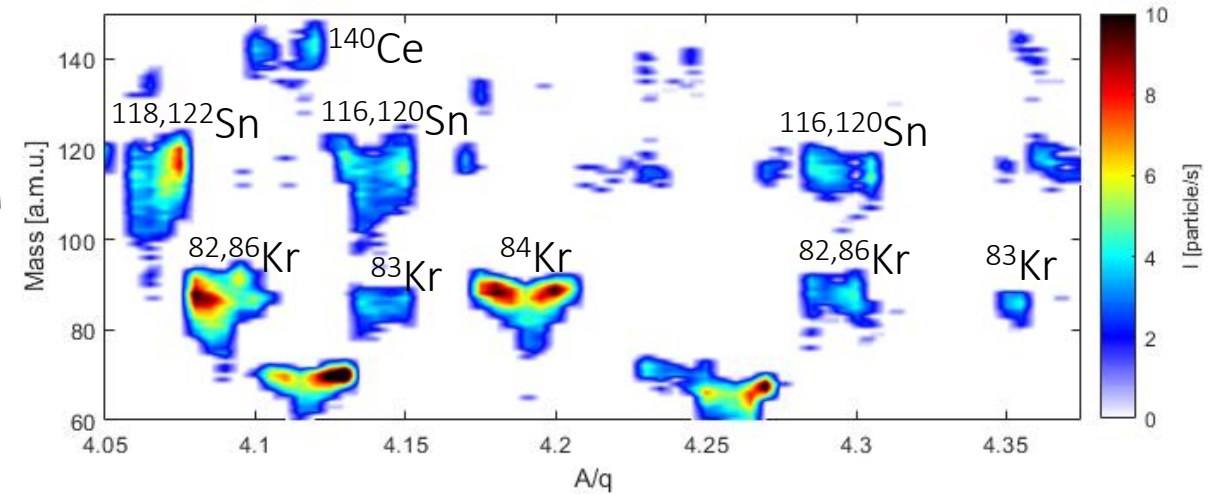


Figure Breeding time = 95 ms ; I_{e^-} = 250 mA.

Axial energy distribution

Technique Variation of REXEBIS extraction potential and monitoring of escaped ions to reconstruct the axial energy distribution.

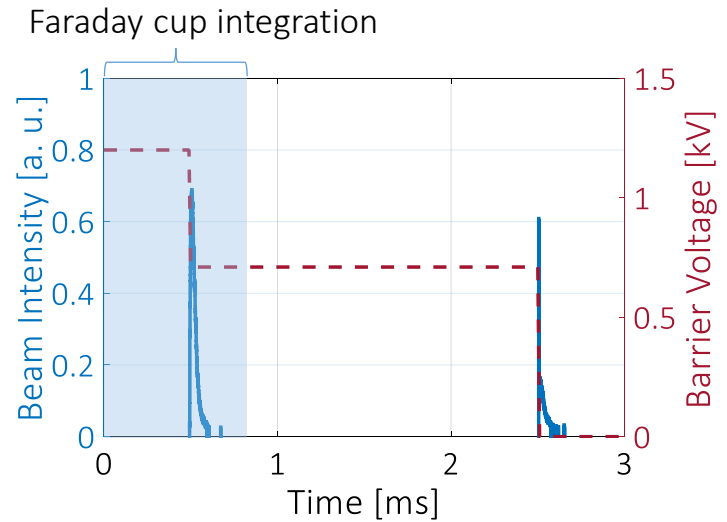


Figure Time-of-Flight measured after the A/q -Separator when gating with the outer barrier.

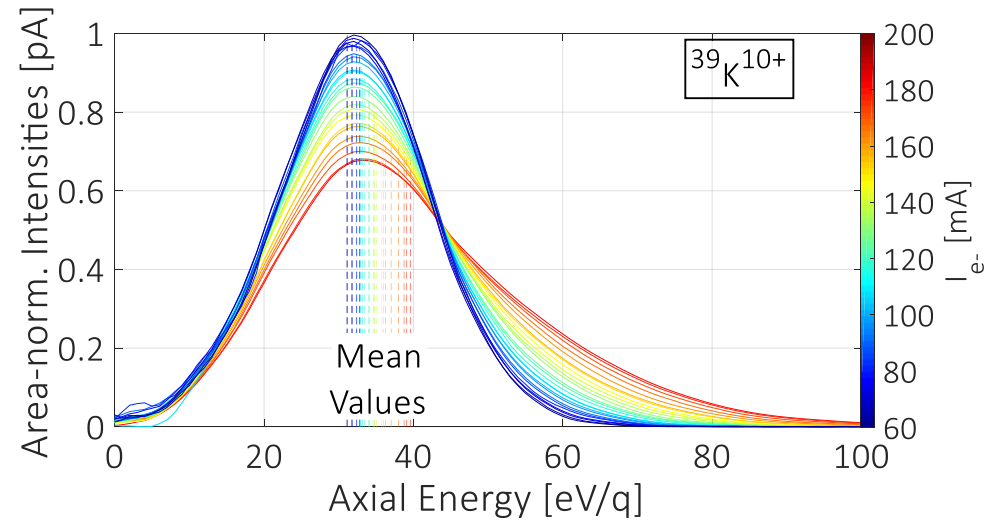


Figure Ionic axial energy distribution measured at REXEBIS extraction, as a function of the electron beam current.

Energy dynamics
$$\frac{dN_i kT_i}{dt} = \left(\frac{dN_i kT_i}{dt} \right)^{\text{Coulomb}} + \left(\frac{dN_i kT_i}{dt} \right)^{\text{Ionisation}} + \sum_j \left(\frac{dN_i kT_i}{dt} \right)^{\text{Transfer}} + \left(\frac{dN_i kT_i}{dt} \right)^{\text{Escape}}$$

Spitzer formalism
$$\Delta E_q^{\text{axial}}(\text{eV}) = \frac{e^3}{16\pi\epsilon_0^2} \left(\frac{m_e}{M_i} \right) \frac{1}{E_e} \left[e \sum_{i=1}^{q-1} \frac{i^2}{\sigma_i^{\text{EI}}} + j_e q^2 \Delta t \right] \quad \text{and} \quad \Delta E_q^{\text{radial}}(\text{eV}) = 2C_\lambda \Delta E_q^{\text{axial}}$$

Slow Extraction

Technique Discretization of the axial energy distribution and solve all $V_{\text{barrier}}(t_i)$ (barrier step-function) to obtain a constant escape rate.

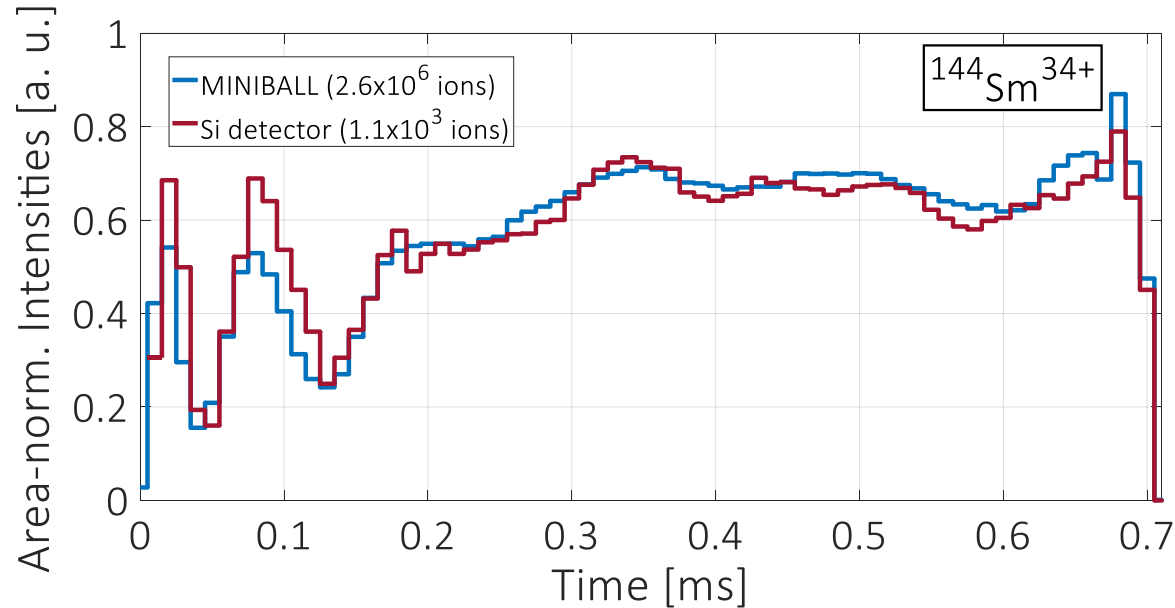


Figure Direct application of inversion formula, comparison between detectors.

Ion energy distribution may be assumed a Maxwell-Boltzmann with 3 DoF: $f(E_i) = \frac{2}{kT_i} \left(\frac{E_i}{\pi kT_i}\right)^{1/2} \exp\left(-\frac{E_i}{kT_i}\right)$

Reduction of contamination via delayed extraction of the beam of interest (high CS) can be improved, notably with higher current density.

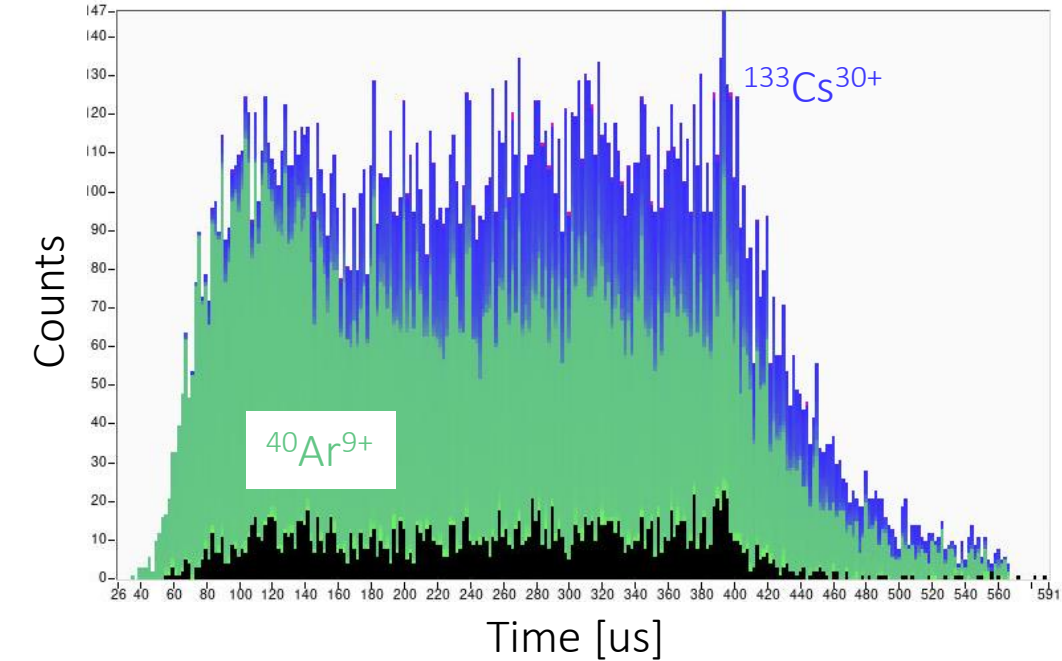
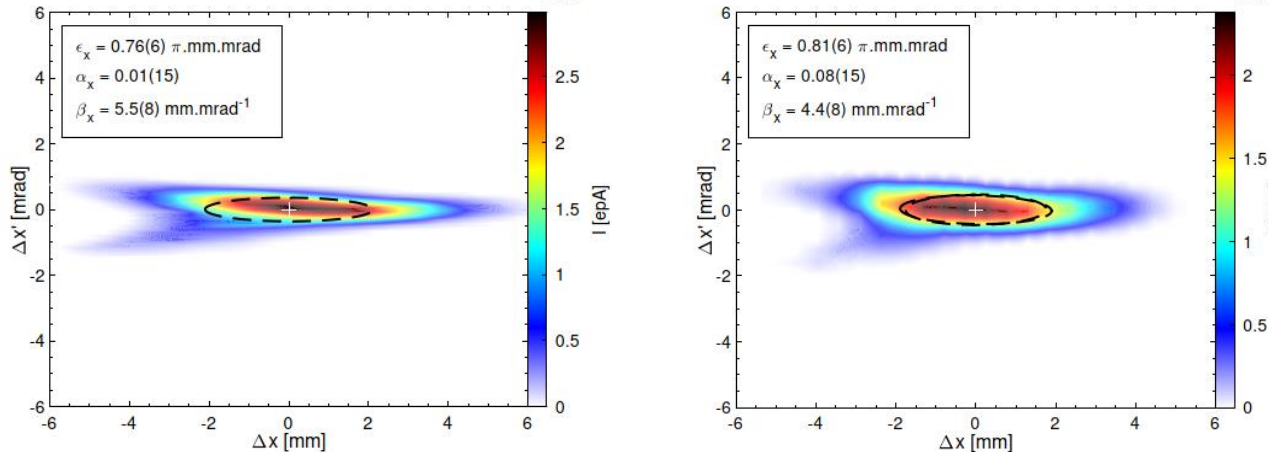


Figure Direct application of inversion formula, on a beam with contaminant.

"Slow Extraction of Charged Ion Pulses from the REXEBIS", N. Bidault, et al., AIP Conf. Proc. 2011 (2018) 070003.

HIE-ISOLDE Transverse beam properties characterization

Experimental setup $^{39}\text{K}^{10+}$ @ 3.82 MeV/u, thin-slits and quadrupoles are used to probe the transverse phase-space for two ranges of intensity.



Figures Double-slit scan using Faraday cup (>10 epA) Silicon detector (<1 efA).

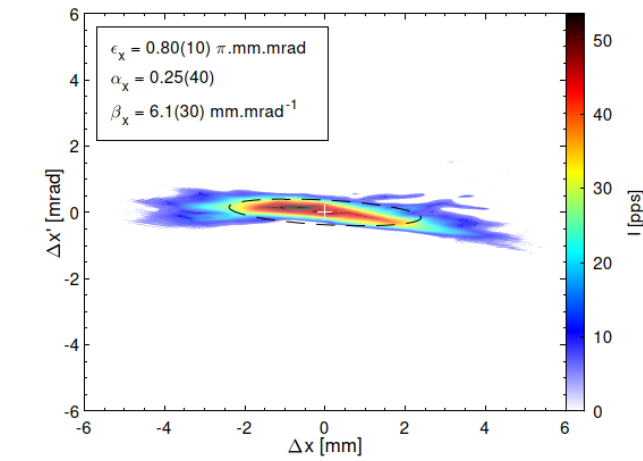
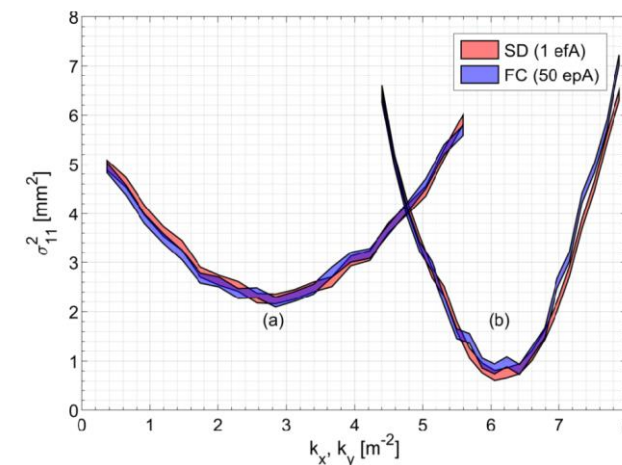
Method

With the quadrupole scan the transverse phase-space is sliced once and rotated.

Result

Validation of the new methodology with very low intensity ion beams.

Tomographic reconstruction possible.



Figures Quadrupole scans for two range of intensity and tomographic reconstruction.

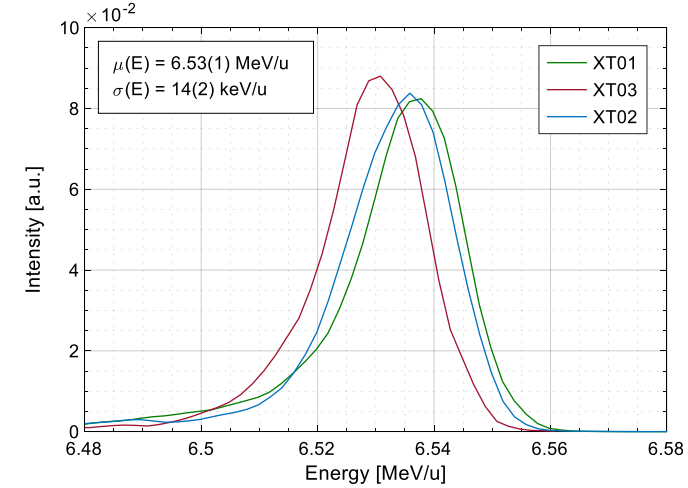
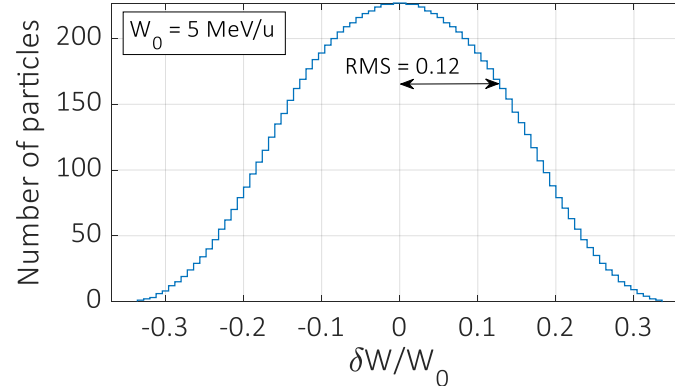
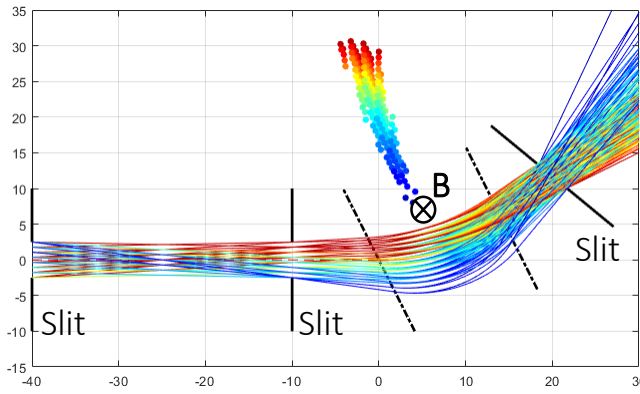
HIE-ISOLDE Beam energy distribution measurement

Technique Use of an HEBT dipole as energy-spectrometer and three vertical slits. Acquisition of beamlet current by a Silicon detector.

Measurements using the three HEBT dipoles confirmed to be similar.

The energy spread derived is overestimated depending on the beam transverse emittance and the spacing between the 1-mm vertical slits.

Proven capability to measure the energy distribution of very low intensity ion beams.



Figures Energy measured using each XT0x dipole.

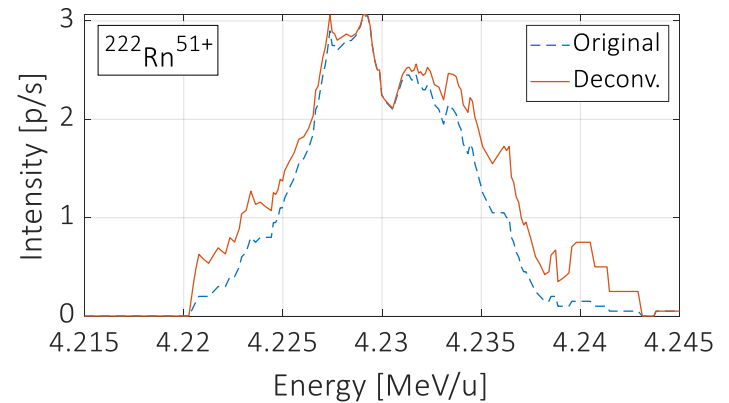


Figure Estimation the inherent spread introduced by the thin slits in the measurement channel and deconvolution on typical energy distribution measured from a RIB.

HIE-ISOLDE Longitudinal phase-space characterization

Experimental setup $^{20}\text{Ne}^{7+}$ @ 6.64 MeV/u, 10 superconducting cavities at nominal accelerating phase, 1 SCC as Buncher at zero-crossing phase.

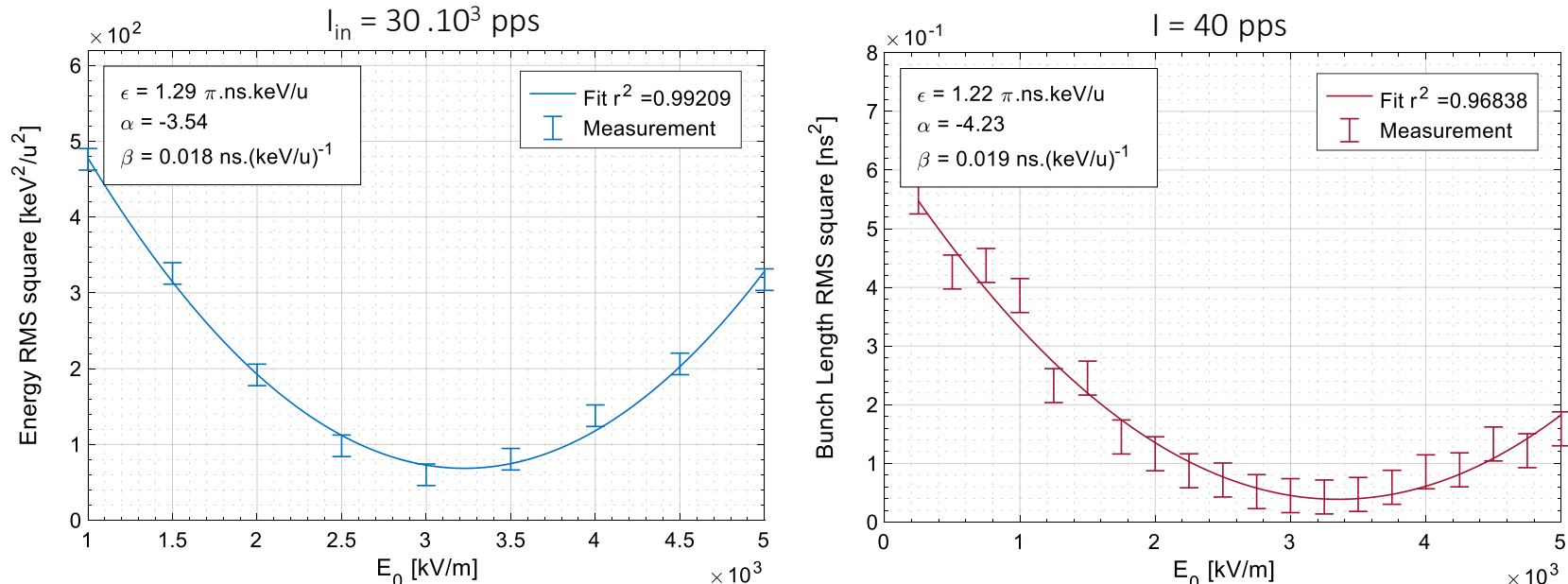
Method

Within beam matrix theory the elements σ_{11} and σ_{22} are quadratic as a function of the gradient of buncher cavity E_0 .

Longitudinal canonical basis: $\begin{pmatrix} \Delta t \\ \Delta W/A \end{pmatrix}$

RF gap: $\begin{pmatrix} 1 & 0 \\ -q\omega_{\text{RF}}E_0 TL_g \sin(\varphi_s) & 1 \end{pmatrix}$

Drift L: $\begin{pmatrix} 1 & -AL \\ 0 & \beta\gamma(\gamma + 1)cW_0 \end{pmatrix}$



Figures Measured energy spread and bunch temporal length as a function of varying E_0 .

Result

Proven capability to characterize the longitudinal phase-space of sub-efA ion beams.

Correlation verified between ToF and energy-spread measurements for the longitudinal phase-space characterization.

Summary

Commissioning of REXEBIS new electron gun

Estimation of jeff

Capability to measure rare contaminants over wide A/q range

Analysis of Coulomb heating

Post-accelerated beam characterization

Consolidation of beam energy measurement technique

Method for probing the transverse beam properties at very low intensity

Method for characterizing the longitudinal phase-space at very low intensity

Thank you for your attention

This work is the result of a collaborative effort involving in particular the following teams at CERN:

ISOLDE Operation (BE-ISO-OP):

Miguel Luis BENITO
Eleftherios FADAKIS
Simon MATAGUEZ
Emiliano PISELLI
Jose Alberto RODRIGUEZ
Erwin Siesling

Beam Physics (BE-ABP):

Gunn KHATRI
Hannes PAHL
Alexander PIKIN
Fredrik WENANDER

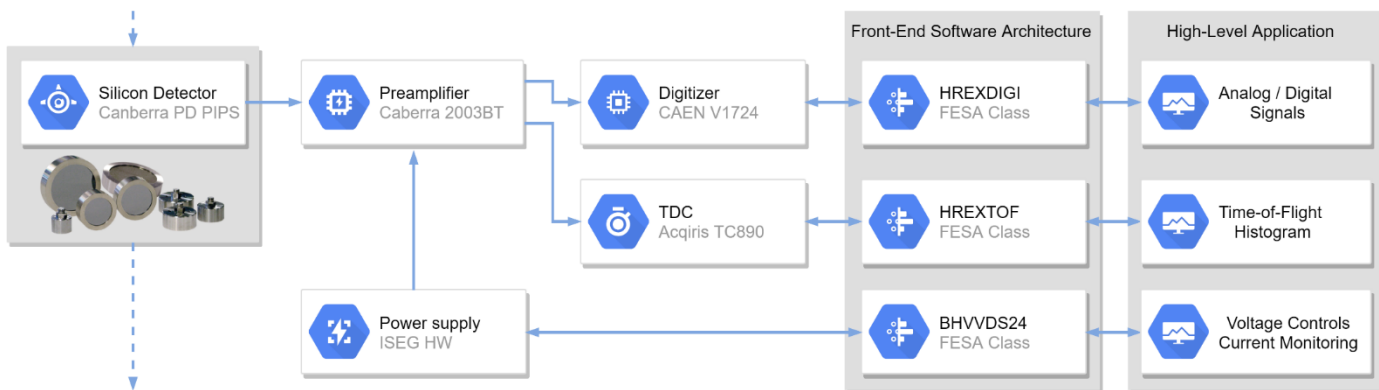
Beam Instrumenation (BI):

William ANDREAZZA
Enrico BRAVIN
Sergey SADOVICH



SAPIENZA
UNIVERSITÀ DI ROMA

Silicon Detector specifications



Figures Diagram of the Silicon Detectors DAQ at HIE-ISOLDE.

Type	Canberra's model	Radius [mm]	Resolution	
			Energy* [keV]	Time [ns]
1	PD50-11-300RM	4.0	11	5
2	TMPD50-16-300RM	4.0	15	0.2
3	PD600-20-300RM	13.8	20	5

Table Basic parameters of 300 μm -thick PD-PIPS detectors used at HIE-ISOLDE (* ^{241}Am , 5.486 MeV alphas).

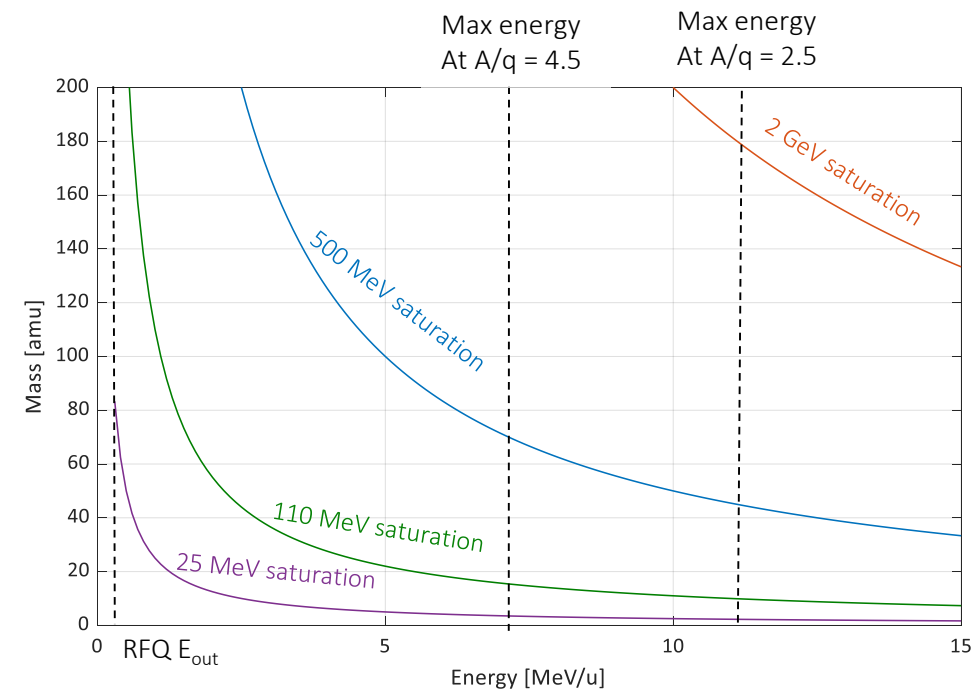


Figure Saturation curves.